Ectopic restriction of DNA repair reveals that UNG2 excises AID-induced uracils predominantly or exclusively during G1 phase

George Sharbeen, Christine W.Y. Yee, Adrian L. Smith, and Christopher J. Jolly

Centenary Institute, the University of Sydney, Sydney NSW 2006, Australia

Immunoglobulin (Ig) affinity maturation requires the enzyme AID, which converts cytosines (C) in *Ig* genes into uracils (U). This alone produces C:G to T:A transition mutations. Processing of U:G base pairs via U N-glycosylase 2 (UNG2) or MutSα generates further point mutations, predominantly at G:C or A:T base pairs, respectively, but it is unclear why processing is mutagenic. We aimed to test whether the cell cycle phase of U processing determines fidelity. Accordingly, we ectopically restricted UNG2 activity in vivo to predefined cell cycle phases by fusing a UNG2 inhibitor peptide to cell cycle–regulated degradation motifs. We found that excision of AID-induced U by UNG2 occurs predominantly during G1 phase, inducing faithful repair, mutagenic processing, and class switching. Surprisingly, UNG2 does not appear to process U:G base pairs at all in *Ig* genes outside G1 phase.

CORRESPONDENCE
Christopher J. Jolly:
c.jolly@centenary.org.au

Abbreviations used: AID, activation-induced deaminase; C, cytosine; RAG2, recombination activating gene 2; SMUG1, single-strand selective monofunctional uracil DNA glycosylase; U, uracil; ugi, U glycosylase inhibitor; UNG2, U N-glycosylase 2.

Rearranged *Ig V(D)J* genes in B cells responding to infections or vaccinations mutate somatically at an ∼1 million-fold higher rate than background mutations (Di Noia and Neuberger, 2007). Rare mutations that improve affinity are selected by competition between B cells to capture antigen via surface expression of their mutated Ig and to present antigen-derived peptides to follicular helper T cells. This rescues the presenting cells from programmed cell death (Allen et al., 2007). Ig class switching, a change from production of IgM to production of IgG, IgA, or IgE, frequently precedes or is concurrent with *V(D)J* point mutation. Class switching occurs via nonhomologous joining of DNA breaks produced in disparate *IgH S* regions, which deletes kilobases of intervening DNA (Jolly et al., 2008; Stavnezer et al., 2008), and changes the Fc portion of the encoded Ig polypeptide without changing antigen specificity or affinity.

Ig mutation and class switching both require activation-induced deaminase (AID; Muramatsu et al., 2000), which directly deaminates cytosine (C) bases in Ig genes, converting them into uracils (U; Di Noia and Neuberger, 2007; Peled et al., 2008). If ignored by DNA repair processes, U deamination causes a C:G to T:A transition mutation to be inherited by one daughter cell. However, AID-induced U are processed by U N-glycosylase 2 (UNG2)–dependent base excision repair (BER) or MutSα-dependent mismatch repair (Rada et al., 2004; Shen et al., 2006). UNG2 (the nuclear isoform of UNG) cleaves the *N*-glycosilic bond in genomic U, leaving the deoxyribose backbone intact. This creates an apyrimidinic (AP) site that is unusable as a template by most DNA polymerases (Di Noia and Neuberger, 2007). AP sites are classically recognized by APE1, which nicks DNA immediately 5′. The original base can then be restored by DNA polymerase β (pol β) and XRCC1/DNA ligase III (Robertson et al., 2009). However, AID-induced BER deviates from this classical pathway, because it generates UNG-dependent *Ig* G:C transversion mutations, probably via translesion DNA polymerases. These are presumed to replicate through AP:G sites created by UNG2, introducing any base opposite the AP site (Diaz and Lawrence, 2005; Jansen et al., 2006; Di Noia and Neuberger, 2007).

The Rockefeller University Press $30.00
J. Exp. Med. Vol. 209 No. 5 965-974
www.jem.org/cgi/doi/10.1084/jem.20112379

The Journal of Experimental Medicine

Class switching is also largely ablated in UNG-deficient cells (Imai et al., 2003; Rada et al., 2004), suggesting that the *Ig S* region DNA breaks that recombine during switching derive from AP sites, possibly via nicking with APE-1 or -2 (Stavnezer et al., 2008).

Several N-glycosylases generate AP sites from damaged DNA bases (not just U), and AP sites also arise spontaneously (Dianov et al., 1992; Robertson et al., 2009), generating thousands of AP sites per cell per day (Nakamura and Swenberg, 1999). BER correctly repairs these AP sites, but mysteriously processes the few extra AP sites introduced by AID plus UNG2 with low fidelity. It has been proposed that the timing of U excision in the cell cycle might explain why AID is mutagenic (Faili et al., 2002; Delbos et al., 2007; Di Noia et al., 2006; Hasham et al., 2010), but definitive evidence is lacking. AID was shown to preferentially induce mutations in G1 phase human BL-2 cells (Faili et al., 2002), and factors involved in gene conversion were shown to preferentially associate with the *Ig*λ locus in G1 phase chicken DT40 cells (Ordinario et al., 2009). However, it is uncertain whether mutation is regulated in these transformed cells exactly as it is in vivo, and the association of repair factors with *Ig* loci does not prove active participation in mutation. Similarly, AID was shown to preferentially induce *IgH* DNA repair foci and DNA breaks in G1 phase class-switching primary B cells (Petersen et al., 2001; Schrader et al., 2007), but these phenomena could reflect either mutagenic or nonmutagenic DNA repair. In any case, the normal relationship between UNG2 activity and the cell cycle is unclear. UNG2 is classically thought to excise U in the vicinity of replication forks (i.e., in S phase; Otterlei et al., 1999; Nilsen et al., 2000; Kavli et al., 2002; Hagen et al., 2008). However, UNG2 activity in HeLa cells peaks in late G1/early S phase and is subsequently negligible (Fischer et al., 2004), suggesting that UNG2 might not process U efficiently in later S phase. UNG2 activity increases by 3–20-fold upon B cell activation (Di Noia et al., 2006; Doseth et al., 2011), and may not subsequently vary through the cell cycle (Schrader et al., 2007). Precise determination of when UNG2 excises AID-induced U would greatly improve our understanding of the mechanism of antibody mutation, and of AID-induced cancer. We reasoned that fusing the uracil glycosylase inhibitor (ugi), from bacteriophage PSB2, to motifs that recruit cell cycle–dependent proteasomal degradation (degrons) would restrict UNG activity to cell cycle phases in which ugi was degraded. Ugi competitively inhibits UNG activity by binding over the catalytic pocket (Mol et al., 1995), but does not inhibit related U *N*-glycosylases such as single-strand selective monofunctional uracil DNA glycosylase (SMUG1; An et al., 2005). By expressing cell cycle–regulated ugi in normal primary B cells, we were able to quantitatively measure the impact of restricting UNG2 activity to distinct cell cycle phases on actual mutation outcomes.

RESULTS AND DISCUSSION

Construction of cell cycle regulated fusion proteins

Amino acids 440–527 from mouse recombination-activating gene 2 (RAG2), 31–120 from human Cdt1, or 2–87 from mouse cyclin B2 were fused to the C termini of the green or orange fluorescent proteins GFP or mKO2 (Fig. 1 A). These peptides (referred to as rag, cdt, and cyc from this point forward) contain destruction (D) box motifs that polyubiquitinate at specific checkpoints in the cell cycle, leading to rapid proteasomal degradation of fused proteins (Gallant and Nigg, 1992; Brandeis and Hunt, 1996; Li et al., 1996; Mizuta et al., 2002; Sakaue-Sawano et al., 2008). In transduced mouse 3T3 fibroblasts, the rag- and cdt-degrons restricted GFP fluorescence to G1 phase cells and a very small subset of cells that appeared to be in G2 or M phases (Fig. 1 B). In contrast, the cyc-degron concentrated GFP fluorescence in post–G1 phase cells (Fig. 1 B). Double transduction revealed a small overlap in accumulation of rag- or cdt-tagged proteins with cyc-tagged proteins, and suggested that all three degrons prevented fusion protein accumulation in early G1 phase cells (Fig. 1 C). Low fluorescence in early G1 was confirmed by time-lapse microscopy (Fig. 1 D and Video 1). It presumably reflected a lag in reaccumulation of tagged proteins after the cessation of degron-directed degradation (Sakaue-Sawano et al., 2008). As expected, the rag- and cdt-degrons directed fusion proteins to the nucleus, whereas the cyc-degron did not (Fig. 1 D; Pines and Hunter, 1994; Corneo et al., 2002; Sakaue-Sawano et al., 2008).

We fused the 85-residue ugi peptide (Di Noia and Neuberger, 2002) to the N terminus of GFP and to GFP-rag, GFP-cdt, and GFP-cyc fusion proteins, and then retrovirally expressed the resulting fusion proteins (ugi-GFP, ugi-GFP-rag, ugi-GFP-cdt, and ugi-GFP-cyc) in C57BL/6 splenocytes stimulated with LPS in vitro. The cell cycle regulation of cdt- and cyc-fusion proteins seemed identical in LPS blasts and 3T3 cells. However, rag-fusion proteins were less stringently regulated in LPS-activated B cell blasts than in 3T3 fibroblasts because ugi-GFP-rag accumulated in a higher proportion of post–S phase LPS blasts than did GFP-rag in 3T3 cells (compare Fig. 1 C and Fig. 2, A and B). Reduced stringency was independent of the presence of the ugi peptide (Fig. 2 B) and was therefore intrinsic to LPS blasts. Pulse-labeling with BrdU confirmed that ugi-GFP-rag was almost absent from S phase LPS blasts, whereas ugi-GFP-cdt expression leaked into early S phase (Fig. 2 A). Nonetheless, overlap in expression of rag- or cdt- and cyc-tagged proteins near the G1/S border was largely caused by the cessation of cyc-directed degradation before detectable incorporation of BrdU. That is, cyc-directed degradation ceased in late G1 phase, before cells had entered S phase (Fig. 2 A).

It was possible that ligation of UNG by ugi-fusions lead to UNG co-degradation when the ugi-fusions were polyubiquitinated. This would create a lag in UNG recovery once tag-induced degradation ceased. To examine this possibility, we performed Western blots for UNG2 on total protein extracts prepared from 3T3 fibroblasts that were 100% transduced with ugi-GFP-rag or ugi-GFP-cyc, and then sorted into GFP^+ and GFP^- populations. We found no evidence for co-degradation of UNG2 with tagged ugi-fusion proteins (Fig. 1 E).

G1 phase UNG2 activity mediates Ig class switching

As would be expected, constitutive ugi-GFP expression greatly reduced in vitro class switching to IgG1 in primary mouse B cells (Fig. 2 C). Switching was similarly reduced when ugi was largely absent in S phase, that is, in cells expressing ugi-GFP-rag or ugi-GFP-cdt (Fig. 2 C). However, class switching was much less reduced in cells expressing ugi-GFP-cyc, in which ugi was expressed from late G1 phase through to completion of replication (Fig. 2 C). The limited ability of ugi-GFP-cyc to inhibit switching was not a result of the cyc-motif interfering with interaction between ugi and UNG, as expression of ugi-GFP-cyc^{Dmut}, which carried two D-box amino acid changes preventing checkpoint ubiquitination (Brandeis and Hunt, 1996; Fig. 2 B, bottom), reduced switching as much as expression of ugi-GFP (Fig. 2 C). Excision of U from a hemifluorescent double-stranded DNA substrate by cell extracts confirmed that both ugi-GFP-rag and ugi-GFP-cyc blocked UNG activity in GFP^{+ve}-transduced B cells (Fig. 2 D).

Because Ig class switching depends on cell proliferation (Hodgkin et al., 1996; Deenick et al., 1999), we also measured switching per cell division (Fig. 2 E). Ugi-GFP-rag, ugi-GFP-cdt, and ugi-GFP-cyc^{Dmut} all inhibited switching per cell division markedly more than control fusion proteins lacking ugi or ugi-GFP-cyc (Fig. 2 E). We therefore explain the ability of ugi-GFP-cyc to partially inhibit switching by overlap of ugi-GFP-cyc accumulation with ugi-GFP-rag (and ugi-GFP-cdt) in late G1 phase and conclude that all of UNG2's contribution to switching occurs in G1 phase. This conclusion is consistent with the detection of DNA damage response foci and DNA breaks in *IgH* loci in G1 phase B cells activated to class switch in vitro (Petersen et al., 2001; Schrader et al., 2007). It is unsurprising because nonhomologous end joining of double-strand breaks, the principal mechanism of

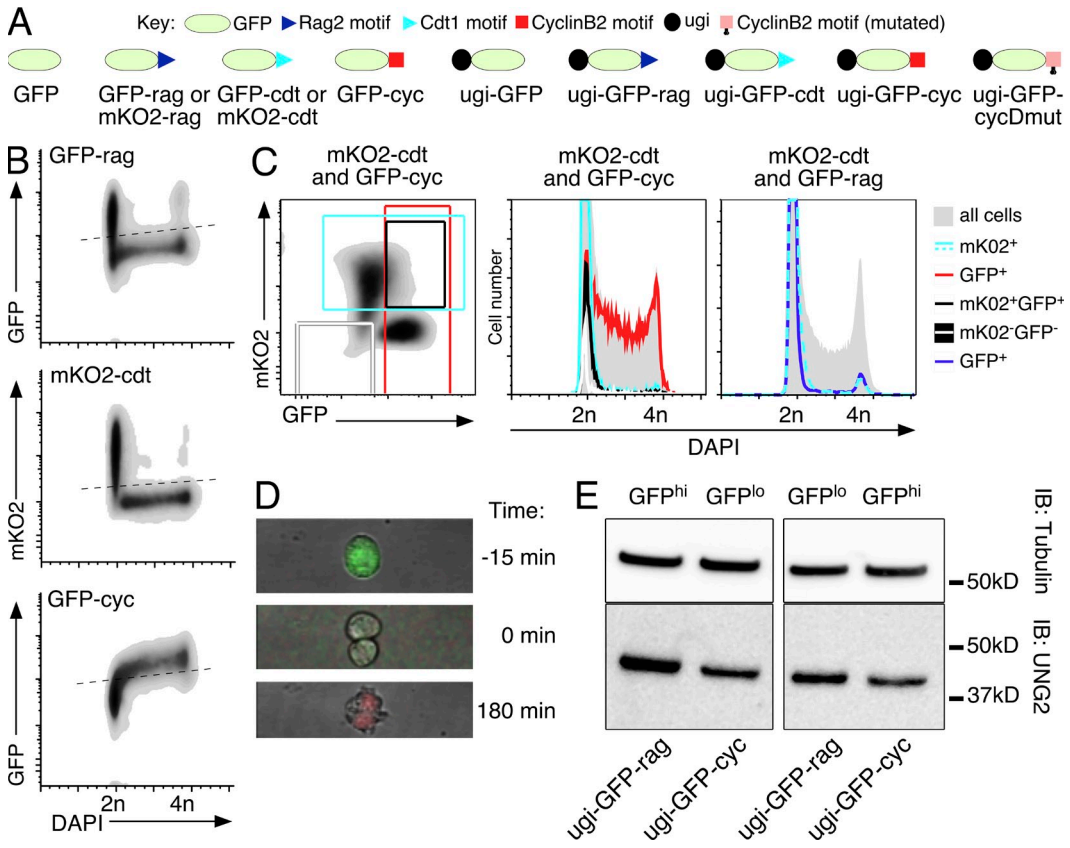

Figure 1. Regulation of fusion protein degradation by cell cycle. (A) Schematic of fusion proteins used in this study. The same symbols for degrons will be used in all figures. (B) Flow cytometric density plots of GFP fluorescence as a function of DNA content (DAPI fluorescence) in NIH-3T3 cultures in which all cells were transduced to express GFP-rag, mKO2-cdt, or GFP-cyc fusion proteins. Dashed lines indicate the approximate boundary of fluorescent and nonfluorescent populations according to nontransduced control cells. (C) The distribution of DNA content in subpopulations of double-transduced NIH-3T3 cells. Cells express mK02-cdt and GFP-cyc (left and middle) or mK02-cdt and GFP-rag (right). The left panel gates populations shown in the middle panel. (D) Images selected from time-lapse (15-min interval) confocal imaging of an NIH-3T3 cell double-transduced to express mKO2-cdt and GFP-cyc, which divided just before T = 0 min. Each image shows summed z-stacks for green and orange fluorescence overlaying a bright-field image. Immediately before cell division (T = −15 min) green fluorescence was intense. Fluorescence reverted to background upon cell division (T = 0 min), and no green or orange fluorescence was detectable above background in the daughter cells until T = 180 min, when orange fluorescence became detectable. (E) Anti-UNG2 Western blot of total protein extracts from 100% transduced 3T3 fibroblasts sorted into GFP$^+$ and GFP$^-$ populations (using gating identical to C). Samples were prestandardized to tubulin by semiquantitative Western blot. Experiments in all panels were performed at least twice.

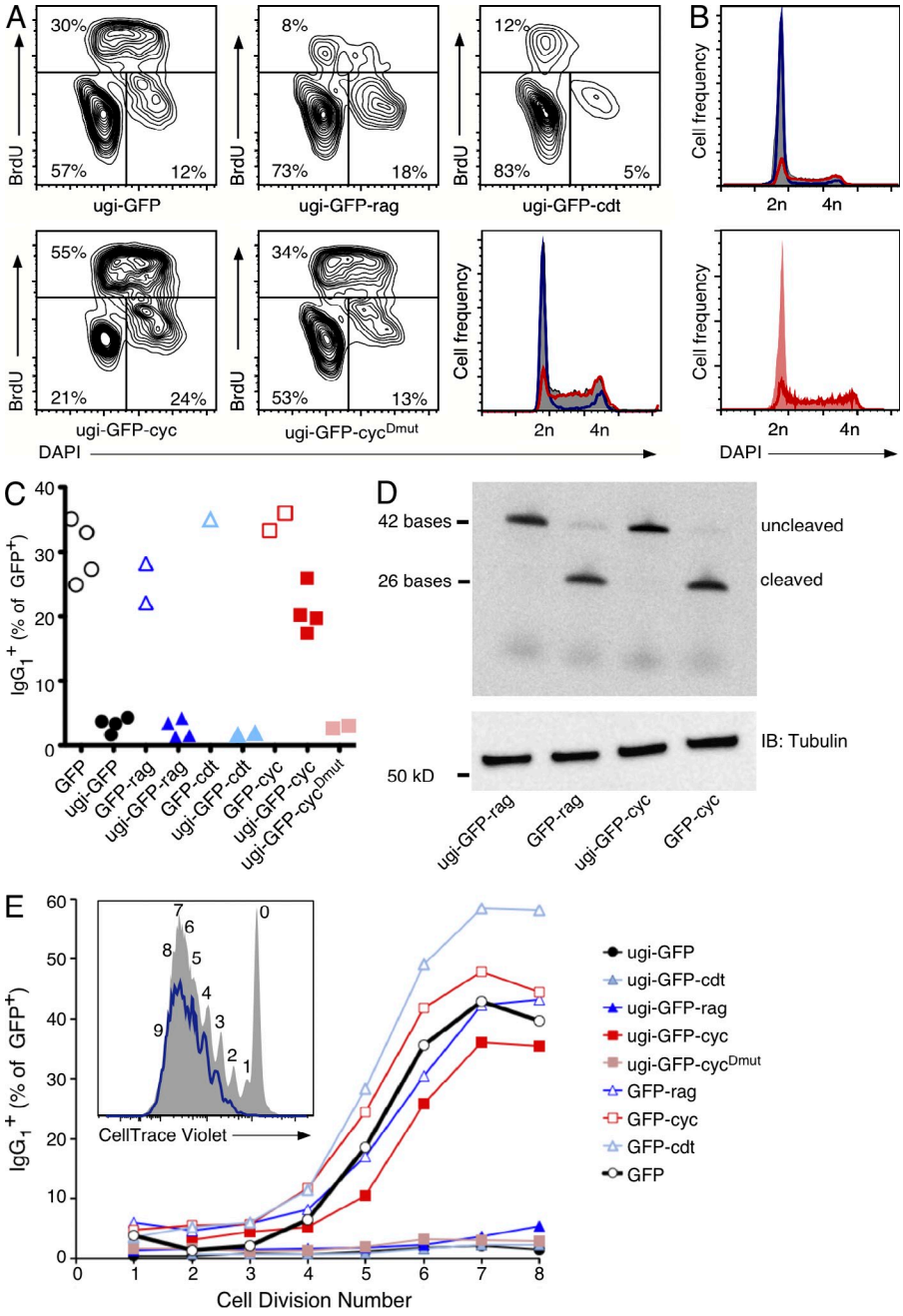

Figure 2. Inhibition of UNG2 outside S phase blocks Ig class switching. (A) Flow cytometric analysis of cell cycle in transduced LPS-activated B cell blasts. Contour plots show BrdU incorporation as a function of DNA content in gated GFP+ cells that were fixed, permeabilized, and stained after a 1-h BrdU pulse (this experiment was performed twice). The fraction of total GFP+ cells encompassed by each gate is indicated. Bottom left gate, G1 phase cells; top gate, S phase cells; bottom right gate, G2/M phase cells. The histogram (bottom right) shows distribution of DNA content in GFP+ cells expressing ugi-GFP (solid gray), ugi-GFP-rag (blue), or ugi-GFP-cyc (red). The vertical scales are arbitrarily adjusted to mimic Fig. 1 C. (B) The distribution of DNA content in GFP+ LPS-activated B cells transduced to express GFP (solid gray), GFP-rag (blue), GFP-cyc (red; top), or ugi-GFP-cyc (bottom) or ugi-GFP-cyc^{Dmut} (solid pink) fusion proteins. The vertical scales are arbitrarily adjusted to mimic Fig. 1 C. (C) Switching from surface IgM to IgG1 expression in transduced B cell blasts. C57BL/6 splenocytes were cultured overnight with bacterial LPS, transduced to express the fusion proteins indicated, and then placed back into culture with LPS+IL-4. 3 d later, cells were surface labeled with APC-conjugated anti-IgG1 antibody. The frequencies of IgG1+ cells in the GFP+ populations, as determined by flow cytometry, are indicated for four independent experiments (some viruses were tested <4 times). (D) U excision activity in GFP+ transduced B cell blasts. 2 d after transduction, whole-cell extracts were prepared from sorted GFP+ B cells activated with LPS. (top) Cleavage of a fluorescent U-bearing oligonucleotide (heteroduplexed to create a U:G base pair, see Table S1) by extracts equivalent to 2 × 10^4 sorted cells (supplemented with 5 units of recombinant APE1 [New England Biolabs] and with anti-SMUG1 antibody PSM1) in a 4-h incubation at 37°C. (bottom) Western blot for tubulin in the same cell extracts. A repeat experiment produced the same results (not depicted). (E) Switching to IgG_1 as a function of cell division number in one experiment. Splenocytes were labeled with CellTrace Violet before culture and transduction. Inset shows the distribution of CellTrace Violet fluorescence for all cells (gray), or GFP^{+ve} cells (thick line) expressing ugi-GFP-rag. The number of divisions each cohort has undergone is indicated by the digits above each cohort peak. Plotted is the percentage of surface IgG_1^+ cells detected in each division cohort of GFP+ cells transduced to express fusion proteins. Symbols as in Fig. 2 C. A repeat experiment produced the same results (not depicted). This experiment is one of the replicates shown in Fig. 2 C.

switch recombination (Jolly et al., 2008), is favored in the G1 phase, when competition with homology-directed repair is reduced (Fukushima et al., 2001).

G1 phase UNG2 activity mediates Ig transversion mutation at G:C base pairs

In contrast to class switching, the cell cycle timing of in vivo Ig point mutation events is unknown. Because no in vitro models completely recapitulate in vivo V(D)J somatic mutation, we used a Switch-HEL (SW_{HEL}) transduction/adoptive transfer model to measure the influence of our fusion proteins on V(D)J point mutation (Sharbeen et al., 2010). SW_{HEL} mice carry a gene-targeted VDJ_H-rearrangement and a transgenic Ig_K gene, together conferring Ig specificity for hen egg lysozyme (HEL). Inactivation of *rag1* or *rag2* in SW_{HEL} mice prevents V(D)J receptor editing, ensuring that all B cells

express identical HEL-specific receptors (Cook et al., 2003). $SW_{HEL}rag1^{-/-}$ splenocytes (simply referred to as SW_{HEL} cells from this point on) were induced into cell cycle using recombinant CD40L ex vivo, and then transduced to express GFP fusion proteins. Sorted GFP^{+ve} cells were injected with appropriate antigen (HEL-conjugated sheep red blood cells) into primed congenic hosts to induce a humoral immune response to HEL dominated by the adoptive SW_{HEL} B cells (Sharbeen et al., 2010). 6 d later, SW_{HEL} VDJ_H-sequences were recovered from immunized mice using flow cytometric sorting of GFP^{+ve}, HEL-binding splenocytes into 96-well plates at 1 cell/well, followed by single-cell PCR. Background mutation in this model (presumably caused by PCR error) is ~1 mutation per 94 sequences (Sharbeen et al., 2010).

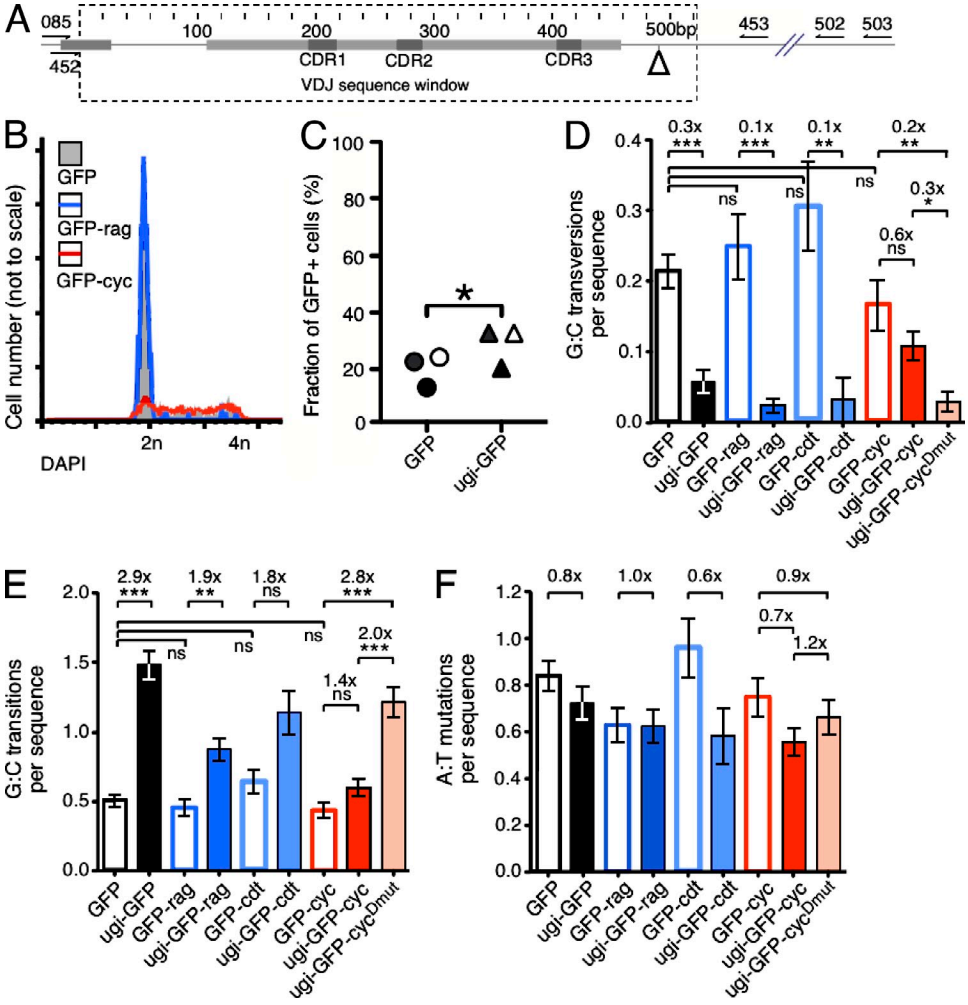

Figure 3. Inhibition of UNG2 in G1 phase inhibits transversion mutation and increases transition mutation at *IgV* G:C base pairs. SW_{HEL} splenocytes were cultured overnight with recombinant CD40L and transduced to express GFP fusion proteins. 2 d later, ≤10^4 sorted GFP$^+$ cells were injected into primed male congenic hosts, along with 10^8 HEL-SRBC. Individual GFP$^+$ cells that bound red fluorescent HEL were recovered from host spleens 6 d after adoptive transfer by flow cytometric sorting into 96-well plates. (A) Map of the SW_{HEL} VDJ_H allele. The dashed box shows the 523-bp window sequenced. VDJ-coding regions are indicated by the gray boxes, with CDRs indicated in darker gray. Nested PCR primers and the sequencing primer (453) are indicated by arrows. The position of a 562bp germline deletion (relative to the wild-type C57BL/6 *IgH* allele) is indicated by "Δ." (B) The distribution of DNA content among GFP$^+$ cells from hosts that received SW_{HEL} cells transduced to express the proteins indicated. Vertical scales are arbitrarily adjusted to mimic Fig. 1 C. (C) Expression of ugi-GFP increases the fraction of cells in post–G1 phase in vivo (ipso facto, it also decreases the fraction of cells in G1 phase). SW_{HEL} splenocytes were transduced with GFP (circles) or ugi-GFP (triangles) and adoptively transferred. 5 d later, the distribution of GFP^{+ve} splenocytes between G1 (2n DNA) and post-G1 (>2n DNA) phases was determined by DAPI fluorescence. The fractions of GFP^{+ve} cells with >2n DNA content from three independent experiments (black, gray and white symbols) are plotted. *, $P < 0.05$, two-tailed paired Student's *t* test. (D–F) The mean number per sequence (±SEM) of transversion mutations at G:C base pairs (D), transition mutations at G:C base pairs (E), or mutations at A:T base pairs (F) detected in single GFP$^+$HEL$^+$ splenocytes transduced to express the proteins indicated by x-axis labels. The total number of hosts, sequences, and mutations contributing to each column are given in Table 1. The multiplier placed above the brackets indicates the change in mutation in ugi$^+$ cells relative to appropriate control cells, accompanied by a significance indicator (according to one-way nonparametric ANOVA combined with Dunn's multiple comparisons) ***, $P < 0.001$; **, $P < 0.01$; *, $P < 0.05$; ns, $P > 0.05$, respectively. None of the A:T mutation means (in F) were significantly different from any other.

Table 1. Summary of mutation in transduced adoptive SW_{HEL} cells.

Transduced cells	Transduced protein	Number of			Number of mutations					
					G		C			
		Hosts	Sequences	Mutations	Tv	Ts	Tv	Ts	A	T
msh2$^{wt/wt}$ SW_{HEL}	GFP	8	398	619	59	114	26	86	260	74
	ugi-GFP	4	208	471	6	147	6	161	113	38
	GFP-rag	4	173	231	26	42	17	37	97	12
	ugi-GFP-rag	5	218	332	3	103	2	87	112	25
	GFP-cdt	2	95	181	21	34	8	27	66	25
	ugi-GFP-cdt	2	65	114	2	28	0	46	27	11
	GFP-cyc	4	175	236	20	45	9	31	109	22
	ugi-GFP-cyc	4	243	307	20	73	6	72	102	34
	ugi-GFP-cyc^{Dmut}	4	141	269	3	90	1	81	68	26
msh2$^{ko/ko}$ SW_{HEL}	GFP	3	152	141	18	38	4	74	6	1
	ugi-GFP	2	101	344	0	115	1	225	0	3
	ugi-GFP-rag	2	72	143	2	44	0	96	0	1
	ugi-GFP-cyc	3	90	91	5	35	0	47	4	0

Table lists the number of host mice that received SW_{HEL} or *msh2*$^{ko/ko}$$SW_{HEL}$ B cells transduced to express the indicated protein, the total number of SW_{HEL} VDJ_H sequences recovered from those hosts, and the sum total of point mutations detected. These mutations are divided into tranversion ("Tv") or transition ("Ts") mutations at G or C, and mutations at A or T, referring to the nontemplate strand. The 523-bp sequence window examined is illustrated in Fig. 3 A.

Cell cycle regulation of the fusion proteins in adoptive B cells in vivo was directly comparable to that seen in cultured 3T3 cells. Notably, rag-tagged GFP was barely detectable outside G1 phase (Fig. 3 B). We also noticed that constitutive expression of ugi slightly increased the proportion of post–G1 phase cells in vivo (Fig. 3 C). Mutation data are summarized in Table 1. We scored mutations in SW_{HEL} cells transduced with GFP-rag, GFP-cdt, or GFP-cyc and observed mostly small and universally nonsignificant ($P > 0.05$) changes in mutation compared with cells expressing GFP alone (Table 1 and Fig. 3 D); thus, controlling for potential nonspecific effects of the fusion tags. Expression of ugi-GFP, ugi-GFP-rag, ugi-GFP-cdt, or ugi-GFP-cyc^{Dmut} all significantly ($P < 0.01$) reduced the frequency of G:C transversion mutations by 73, 91, 90, or 89% compared with the appropriate GFP, GFP-rag, GFP-cdt, or GFP-cyc control, respectively (Table 1 and Fig. 3 D). In contrast, ugi-GFP-cyc reduced G:C transversion mutations by only 35% ($P > 0.05$) compared with the GFP-cyc control (Fig. 3 D). These data strongly suggest that UNG2 activity in G1 phase is responsible for G:C transversion mutations because the ability of ugi-GFP-cyc to partially inhibit G:C transversion mutation is readily explained by accumulation overlap with ugi-GFP-rag and ugi-GFP-cdt in late G1 phase. If coordination of UNG2 activity with the replication fork was critical for the generation of G:C transversion mutations, then ugi-GFP-cyc and not ugi-GFP-rag or -cdt would have had the greatest impact on G:C transversion frequency.

G1 phase UNG2 activity predominantly mediates the correct repair of Ig U:G base pairs

Our aforementioned analyses indicate that only G1 phase UNG2 activity is mutagenic in B cells. However, UNG2 would also be expected to induce the correct repair of U in activated B cells. Indeed, inactivation of the *ung* gene increases the frequency of Ig transition mutations at G:C base pairs in excess to the reduction in G:C transversion mutation, which suggests that processing of AID-induced U:G base pairs by UNG2 leads to significant restoration of C:G base pairs (Storb et al., 2009). Our data clearly recapitulate the phenomenon: the SW_{HEL} VDJ_H genes in cells expressing ugi-GFP or ugi-GFP-cyc^{Dmut} contained 2.9× or 2.8× as many transition mutations at G:C as cells expressing GFP or GFP-cyc, respectively (Fig. 3 E). We interpret this to represent removal in UNG-proficient cells of almost two-thirds of the G:C transitions found in cells lacking UNG activity, presumably via classical BER or by a preference for translesion bypass to insert G opposite AP sites. However, only ∼16% of the transitions removed via UNG2 are converted into G:C transversion mutations (G:C transversions/sequence lost by constitutively blocking UNG, divided by G:C transitions/sequence gained by constitutively blocking UNG = [(59 + 26)/398]/[(6 + 6)/208] = 0.16/0.98 = 16%; numbers from first two rows in Table 1). This implies restoration of U in place of 84% of the AP sites generated by UNG2 from AID-induced U in the VDJ_H regions of UNG-proficient SW_{HEL} cell. The reduction in G:C transversion mutation induced by G1-restricted ugi-GFP-rag or ugi-GFP-cdt, which was at least equivalent to that induced by constitutive ugi-GFP (Fig. 3 D), was associated with a smaller increase in G:C transition mutation of only 1.8× to 1.9× relative to cells expressing GFP-rag or GFP-cdt (Fig. 3 E). Thus, ugi expression restricted to G1 phase almost ablated mutagenic processing of U via UNG2, but seemed to inhibit correct repair to a much lesser extent than constitutive ugi expression. Because UNG2

was reported to excise U:A base pairs during postreplicative DNA repair (Nilsen et al., 2000), it was initially tempting to conclude that UNG2 induces correct repair when it processes AID-induced U:G base pairs in S phase, possibly by a combination of BER and homology-directed DNA repair (Hasham et al., 2010; Saribasak et al., 2011). Ugi-GFP-cyc blocked UNG activity in S phase cells (Fig. 2 D), but expression of ugi-GFP-cyc increased G:C transition mutation a mere 1.4× relative to cells expressing GFP-cyc (Fig. 3 E), indicating that both mutagenic and correct processing of U:G base pairs were largely unaffected by inhibition of UNG2 outside G1 phase. We considered the possibility that expression of ugi-GFP-cyc could lead to preferential processing of U:G base pairs by mismatch repair, removing U that would otherwise produce transition mutations. We therefore expressed some ugi-fusion proteins in adoptive *msh2*$^{-/-}$ *SW*$_{HEL}$ B cells and observed the same trends found in *msh2*$^{wt/wt}$ cells, i.e., that expression of ugi-GFP, ugi-GFP-rag, or ugi-GFP-cyc increased the mean frequency of G:C transition mutations 4.6×, 2.6×, or 1.2×, respectively, relative to cells expressing GFP alone (Table 1). These findings indicate that inhibition of UNG2 in S phase had little impact on processing of AID-induced U even in the complete absence of MutSα. We deduce that excision of AID-induced U by UNG2 in G1 phase induces predominantly correct repair, alongside mutagenic processing, whereas in S phase, UNG2 excises few or no AID-induced U at all. This is surprising, because many U ignored by UNG2 in G1 phase presumably persist into S phase, particularly in MutSα-deficient cells. This is because the only other activity likely to be able to efficiently induce repair of U:G base pairs, SMUG1, removes at best a minority of the AID-induced U left unprocessed by UNG2 or MutSα (Di Noia et al., 2006).

In theory, our fusion approach provides the unique ability to tightly restrict the activity of any biochemical pathway to predefined cell cycle phases, provided an inhibitory peptide or protein able to inhibit the pathway of interest is available. We originally fused our peptides to GFP merely to track expression, but subsequently found the inclusion of GFP-like proteins in our constructs to be essential, as direct fusion of the rag- or cyc-peptides to the C-terminus of ugi-produced proteins that were unable to inhibit UNG2 activity, and which were poorly regulated by cell cycle (unpublished data). GFP may have isolated the ugi peptide from the regulatory peptides, preventing each from interfering with the function of (or denaturing) the other.

Our data show that UNG2 excises AID-induced U from *Ig* genes largely or exclusively in G1 phase, consistent with reports that AID targets *Ig* genes in G1 phase in transformed B cell lines (Faili et al., 2002; Ordinario et al., 2009). This does not imply that subsequent mutation steps also occur in G1 phase. Indeed, persistence of UNG-induced AP sites into S phase may be necessary for conversion of an AP site into a permanent G:C transversion mutation. Accordingly, we propose that nicking by APE predominantly determines whether UNG2 U excision is mutagenic. Most of the time, AID/UNG2-induced AP sites are presumably 5′-nicked by APE1 or APE2, but excising and subsequent processing by pol β (the rate-limiting step in classical BER) are insufficiently rapid to prevent some intact and nicked AP sites from accumulating (Nakamura and Swenberg, 1999). In the case of *Ig* S regions, where deamination is dense (Xue et al., 2006), accumulation of nicked AP sites in the G1 phase probably creates staggered double-strand breaks that divert repair from BER to nonhomologous end joining, causing G1 phase class switching (Guikema et al., 2007; Wu and Stavnezer, 2007). In the case of *VDJ*-regions, nicking by APE would be expected to divert from mutagenic translesion synthesis toward classical BER, within G1 phase, and could explain the ∼84% preference we observed for UNG2 to induce reversion of U:G base pairs to C:G base pairs. A minority of AP sites is not nicked by APE1 and persist (Nakamura and Swenberg, 1999), or may be processed by MRN instead (Yabuki et al., 2005). AP sites that persist into S phase without nicking inhibit DNA replication and are likely to induce translesion bypass (Hevroni and Livneh, 1988). Thus, the later in G1 phase UNG2 excises U, the more likely unprocessed AP sites will persist into S phase and recruit translesion bypass. This argument can explain why ugi-GFP-rag and ugi-GFP-cdt induced a 35% lower increase in G:C transitions than did ugi-GFP or ugi-GFP-cyc^{Dmut} (Fig. 3 E), because UNG2 activity in early G1 phase (when ugi-GFP-rag and ugi-GFP-cdt accumulation was below detection; Fig. 1, C and D) would create the AP sites least likely to persist un-nicked through to S phase. Once an AP site has been replicated in S phase, it seems likely from our data that the mutation may be fixed via classical BER in the next G1 phase, which has an ∼84% chance of introducing a base complementary to the mutated base introduced in the previous S phase.

Our data surprisingly reveal that when cells enter S phase, processing of *Ig* U:G base pairs by UNG2 rarely occurs, even though nuclear UNG appears to be abundant (Schrader et al., 2007) and supposedly engaged in excision of U misincorporated opposite A (Nilsen et al., 2000). It is reasonable to postulate from our data that processing by UNG2 of spontaneous or AID-induced U:G base pairs might be restricted to G1 phase in all genes, not just the *Ig* locus. The ability of constitutive ugi to reduce the fraction of cells in G1 phase in vivo is consistent with this notion (Fig. 3 C). However, the damage AID induces in "off-target" genes is lethal in the absence of the homology-directed repair factor XRCC2, implying that AID might induce S phase breaks in these off-target genes (Hasham et al., 2010). This can be reconciled with our data by the interesting possibility that off-target S phase breaks are not the result of UNG2 activity, but instead arise via other activities such as SMUG1 or MutSα. Indeed, the Mutsα subunit MSH2 plays a major role in preventing AID-induced point mutations in off-target genes (Liu et al., 2008). On the other hand, S phase U excision need not necessarily be required to induce S phase homology-directed repair because the persistence into S phase of AP

sites or nicked AP sites generated in off-target genes via G1 phase AID and UNG2 activity may be sufficient to induce replication fork remodeling and homologous recombination.

It is possible that G1 phase restricted U excision occurs in *Ig* genes because AID and UNG2 act in concert as part of a complex whose combined activity is restricted to G1 phase (e.g., via co-association with RPA; Chaudhuri et al., 2004; Hagen et al., 2008). In any case, the apparent irrelevance of S phase UNG2 to antibody mutation implies that any *Ig* C that AID does deaminate in S phase produces G:C transition mutations, is processed correctly by UNG2-independent BER, or is excised by mismatch repair machinery, which would prevent a G:C transition mutation from arising only if mismatch excision occurred before encounter with a replication fork.

MATERIALS AND METHODS

Chemicals. Unless otherwise stated, chemicals were purchased from Sigma-Aldrich and antibodies used for flow cytometry were purchased from BD. Antibodies used for Western blotting were affinity-purified rabbit polyclonal anti-UNG2 (Sigma-Aldrich), mouse monoclonal anti-tubulin (IgG1 Clone B-5-1-2; Santa Cruz Biotechnology), and horse radish peroxidase–conjugated secondary polyclonal antibodies (Millipore).

Mice. Male C57BL/6 host mice were purchased from Animal Resources Centre (Canning Vale, Western Australia) and were used in experiments when 8–12 wk old. SW_{HEL}, $msh2^{ko/ko}$, and $rag1^{ko/ko}$ donor mice, all from a C57BL/6 background (Cook et al., 2003; Sharbeen et al., 2010), were bred and maintained under SPF conditions in the Centenary Animal Facility. Mouse experiments were approved and monitored by the University of Sydney Animal Ethics committee in accordance with the New South Wales Animal Research Act (1985).

Production of plasmids and retroviruses. Sequences for cloning into plasmids were generated by PCR using Phusion DNA polymerase (Finnzymes) according to the manufacturer's instructions. The primers and templates used are listed in Table S1. Fusion protein sequences were assembled into retroviral vector plasmids derived from pMiG in which the internal ribosome entry site had been deleted (Sharbeen et al., 2010). Constructs were assembled by conventional ligation of restriction digested DNA ends using enzymes from New England Biolabs, by heteroduplexing separate PCR products to create hybrid products with 4-base overhangs compatible with restriction enzyme–cleaved vectors, or by recombination overlap PCR (Holst et al., 2006), followed by conventional restriction digestion and ligation or by homology-mediated ligation using an InFusion 2.0 kit (Takara Bio Inc.). The sequences of all fusion proteins were verified by fluorescent Sanger sequencing (Australian Genome Research Facility, Brisbane, Australia). Ecotropic retroviral supernatants were produced by co-transfecting near-confluent HEK293 cells (in 75 cm^2 flasks) using Lipofectamine 2000 (Invitrogen) with 15 µg pMiG-derived plasmid plus 15 µg pCL-Eco helper plasmid (Imgenex). After culture for 48 h at 32°C in B cell medium (Sharbeen et al., 2010), culture supernatants were filtered and stored at −70°C.

Transduction of cells. Log phase mouse NIH-3T3 fibroblasts were transduced by adding thawed retroviral supernatants supplemented with 8 µg/ml polybrene to the culture medium. GFP^{+ve} (488 nm laser, 530 ± 15 nm emission) and/or $mKO2^{+ve}$ (488 nm laser, 575 ± 13 nm emission) cells were purified ≥48 h later by one or more rounds of flow cytometric sorting using a FACS-Aria II machine (BD). Primary mouse splenocytes were purified as previously described (Sharbeen et al., 2010) and activated overnight by 37°C culture at 10^6 cells per ml in B cell medium (Sharbeen et al., 2010) supplemented with 40 µg/ml *Salmonella typhosa* LPS. LPS-activated splenocytes were "spinfected" (1,100 *g*, 45 min, 20°C) with 2×-diluted retrovirus supernatants in the presence of 8 µg/ml polybrene, washed, then incubated for a further 3 d in medium containing LPS plus 20ng/ml recombinant mouse IL-4 (BD Biosciences) to induce switching to IgG_1 (Cook et al., 2003). Primary $SW_{HEL}rag1^{-/-}$ splenocytes were purified and activated overnight by culture with recombinant CD40L as described (Sharbeen et al., 2010), transduced by spinfection, washed, then incubated for an additional 2 d in activating medium. GFP^{+ve} cells were then purified by flow cytometric sorting as above, mixed with HEL-SRBC prepared as previously described (Sharbeen et al., 2010), and injected via a tail vein into 8–12-wk-old male C57BL/6 hosts that had been primed i.p. with 10^8 SRBC 5–7 days earlier. Each host received ≤10^4 GFP^{+ve} cells, along with 10^8 HEL-SRBC in a bolus of 0.25–0.5 ml B cell medium.

Time-lapse microscopy. Transduced NIH-3T3 cells were grown on Laboratory-Tek II 4-well chambered cover glasses (Nunc) to a confluence of ∼50%. Cells were imaged over a 16-h period at 15 min intervals using a Leica SP500 confocal microscope in a humidified, 37°C chamber with 5% CO_2. Bright field and cross-compensated fluorescence images (GFP: 488 nm laser, 500 ± 10 nm emission; mKO2, 561 nm laser, 590 ± 20 nm emission) were collected at each time point using auto-focus. Data were analyzed using Volocity software (PerkinElmer) and exported as false color fluorescence z-stacks superimposed on bright field images.

Measurement of cell cycle. BrdU was incorporated into the DNA of replicating cells using the APC BrdU Flow kit (BD) according to the manufacturer's instructions, with a 1-h BrdU pulse before harvesting cells. Incorporated BrdU was detected in fixed cells with an APC-conjugated anti-BrdU antibody according to the supplier's instructions, followed by staining of DNA with DAPI as described in the following section. An LSR II flow cytometry machine (BD) was then used to collect cell fluorescence caused by GFP (488 nm laser, 525 ± 25 nm emission), APC (633 nm laser, 670 ± 15 nm emission), and DAPI (407 nm laser, 440 ± 20 nm emission). Cytometry data were analyzed using FlowJo software (Tree Star Inc.).

Preparation of cell extracts, Western blot analysis, and U excision assay. Total protein extracts for Western blot were prepared using commercial cell lysis buffer (20 mM Tris-HCl, 150 mM NaCl, 1 mM Na_2EDTA, 1 mM EGTA, 1% Triton, 2.5 mM sodium pyrophosphate, 1 mM β-glycerophosphate, 1 mM Na_3VO_4, 1 µg/ml leupeptin, 100 µg/ml AEBSF, 100 µg/ml PMSF, 1 µg/ml Pepstatin; Cell Signaling Technology) according to the manufacturer's instructions. Whole-cell protein extracts for activity assays were prepared as previously described (Di Noia and Neuberger, 2002), with the following exceptions: snap-frozen cells were lysed directly into activity assay buffer (20 mM Tris-HCl, 1 mM EDTA, 1 mM DTT, 60 mM NaCl, 0.5 mg/ml BSA, 100 µg/ml AEBSF, 100 µg/ml PMSF, 1 µg/ml Pepstatin, pH 8.0) by 10 sonication pulses of 15 s each. Western blots were conducted as previously described (Sharbeen et al., 2010). UDG activity assays were conducted as previously described (Di Noia et al., 2007), with the exceptions that they were performed in the assay buffer of Doseth et al. (2011) and the incubation period was increased to 4 h. All activity assays included excess PSM1, a neutralizing anti-SMUG1 antibody donated by G. Slupphaug (Norwegian University of Science and Technology, Trondheim, Norway; and New England Biolabs).

Measurement of in vitro class switching. For analysis of switching per cell division, purified splenocytes were labeled with CellTrace Violet (Invitrogen), as described by the supplier, before activation and transduction. After 3 d posttransduction culture with LPS plus IL-4, ice-cold splenocytes were stained for surface IgG_1-expression using PerCP-conjugated anti–mouse IgG_1 antibody (clone X56; BD) diluted in PBS (Astral Scientific) supplemented with 0.1% BSA (Bovogen Biologicals) and 0.02% sodium azide, and washed twice. CellTrace Violet-labeled cells were not fixed before flow cytometric analysis. All other cells were fixed for 10 min in the dark at room temperature in 10% neutral buffered formalin (Sigma-Aldrich), washed twice with PBS, and then incubated for 0.5 h at 37°C in the dark with 10 µg/ml DAPI in PBS containing 0.1% Nonidet P-40 (Sigma-Aldrich), 0.1% BSA, 20 µg/ml RNase A, 0.02% azide, and 2 mM EDTA. An LSR II machine

was then used to analyze cell fluorescence caused by GFP (488 nm laser, 525 ± 25 nm emission), mKO2 (561 nm laser, 582 ± 8 nm emission), PerCP (488 nm laser, 695 ± 20 nm emission), and DAPI or CellTrace Violet (407 nm laser, 440 ± 20 nm emission). Cells alive at the time of fixing were defined by a DAPI fluorescence peak area versus peak height gate that incorporated single cells with 2n to 4n DNA content. Live CellTrace Violet–labeled cells were defined by exclusion of 0.1 μg/ml propidium iodide (488 nm laser, 582 ± 8 nm emission).

Measurement of in vivo SW_{HEL} VDJ mutation. 6 d after adoptive transfer, individual transduced SW_{HEL} B cells were recovered from the spleens of congenic hosts into individual wells of 96-well PCR plates (Bio-Rad Laboratories) as GFP^{+ve} cells labeled with Alexa Fluor 647–conjugated HEL (Sharbeen et al., 2010). After cell lysis and protein digestion, the VDJ_H-region of the single SW_{HEL} allele present in each cell was amplified by nested PCR using primers 85 and 503 for primary PCR and primers 452 and 502 for secondary PCR (Table S1), as described (Sharbeen et al., 2010). The PCR products from ≤60 wells per host in which amplification was successful were sequenced by Macrogen using primer 453 (Table S1). Mutations were collated in a window spanning nucleotides 17–539, counting from the translation start ATG codon as bases 1–3.

Statistical analysis of mutation data. For each fusion protein tested, transduced cells were transferred to multiple adoptive hosts (Table 1), and ≤60 cells from each host were sequenced. We previously determined that this approach minimized the need to cull potentially clonal mutations from our mutation databases (Sharbeen et al., 2010). We avoided culling because this technique inevitably overcompensates for clonality by removing mutations at hotspots that genuinely arose independently, especially in $msh2^{-/-}$ cells (Rada et al., 2004). Sequences from multiple hosts were pooled (to further reduce the potential influence of clonality) and unit numbers of mutations per sequence were used to perform nonparametric one-way ANOVA (Kruskall-Wallis tests) using Prism (version 5.0d for Mac OS X; GraphPad Software). Dunn's multiple comparison tests were used to determine whether differences between all pairs were significant. Only differences between experimentally appropriate pairs are indicated in Fig. 3. For instance, the significant difference in G:C transversion mutation between cells expressing GFP versus ugi-GFP-rag is not shown in Fig. 3, because it is not an appropriate comparison.

Online supplemental material. Video 1 shows a time-lapse video of fluorescence caused by mKO2-cdt and GFP-cyc in a double-transduced 3T3 cell before and after its division into two daughter cells. Table S1 shows sequences of oligonucleotide primers used to make fusion protein constructs, amplify and sequence SWHEL alleles, or perform UDG assays. Online supplemental material is available at http://www.jem.org/cgi/content/full/jem.20112379/DC1.

We thank the Centenary Institute Animal Facility for mouse husbandry, Robert Salomon and Steven Allen for cell sorting, Andrew Franklin and Wolfgang Weninger for their critiques of this manuscript, and Geir Slupphaug for donating SMUG1-neutralising antibody (PSM1).

This research was funded by project grants to C.J. Jolly from the National Health and Medical Research Council (512134 and 1012291) and Cancer Council NSW (RG-09-24), and by postgraduate research scholarships to G. Sharbeen from the Australian Federal Government and the Cancer Institute NSW.

The authors have no conflicts of interest to declare.

Submitted: 11 September 2011
Accepted: 14 March 2012

REFERENCES

Allen, C.D., T. Okada, H.L. Tang, and J.G. Cyster. 2007. Imaging of germinal center selection events during affinity maturation. *Science*. 315:528–531. http://dx.doi.org/10.1126/science.1136736

An, Q., P. Robins, T. Lindahl, and D.E. Barnes. 2005. C —> T mutagenesis and gamma-radiation sensitivity due to deficiency in the Smug1 and Ung DNA glycosylases. *EMBO J.* 24:2205–2213. http://dx.doi.org/10.1038/sj.emboj.7600689

Brandeis, M., and T. Hunt. 1996. The proteolysis of mitotic cyclins in mammalian cells persists from the end of mitosis until the onset of S phase. *EMBO J.* 15:5280–5289.

Chaudhuri, J., C. Khuong, and F.W. Alt. 2004. Replication protein A interacts with AID to promote deamination of somatic hypermutation targets. *Nature*. 403:992–998. http://www.ncbi.nlm.nih.gov/pubmed/15273694

Cook, A.J.L., L. Oganesian, P. Harumal, A. Basten, R. Brink, and C.J. Jolly. 2003. Reduced switching in SCID B cells is associated with altered somatic mutation of recombined S regions. *J. Immunol.* 171:6556–6564.

Corneo, B., A. Benmerah, and J.P. Villartay. 2002. A short peptide at the C terminus is responsible for the nuclear localization of RAG2. *Eur. J. Immunol.* 32:2068–2073.

Deenick, E.K., J. Hasbold, and P.D. Hodgkin. 1999. Switching to IgG3, IgG2b, and IgA is division linked and independent, revealing a stochastic framework for describing differentiation. *J. Immunol.* 163:4707–4714.

Delbos, F., S. Aoufouchi, A. Faili, J.C. Weill, and C.A. Reynaud. 2007. DNA polymerase eta is the sole contributor of A/T modifications during immunoglobulin gene hypermutation in the mouse. *J. Exp. Med.* 204: 17–23. http://dx.doi.org/10.1084/jem.20062131

Di Noia, J., and M.S. Neuberger. 2002. Altering the pathway of immunoglobulin hypermutation by inhibiting uracil-DNA glycosylase. *Nature*. 419:43–48. http://dx.doi.org/10.1038/nature00981

Di Noia, J.M., and M.S. Neuberger. 2007. Molecular mechanisms of antibody somatic hypermutation. *Annu. Rev. Biochem.* 76:1–22. http://dx.doi.org/10.1146/annurev.biochem.76.061705.090740

Di Noia, J.M., C. Rada, and M.S. Neuberger. 2006. SMUG1 is able to excise uracil from immunoglobulin genes: insight into mutation versus repair. *EMBO J.* 25:585–595. http://dx.doi.org/10.1038/sj.emboj.7600939

Di Noia, J.M., G.T. Williams, D.T. Chan, J.M. Buerstedde, G.S. Baldwin, and M.S. Neuberger. 2007. Dependence of antibody gene diversification on uracil excision. *J. Exp. Med.* 204:3209–3219. http://dx.doi.org/10.1084/jem.20071768

Dianov, G., A. Price, and T. Lindahl. 1992. Generation of single-nucleotide repair patches following excision of uracil residues from DNA. *Mol. Cell. Biol.* 12:1605–1612.

Diaz, M., and C. Lawrence. 2005. An update on the role of translesion synthesis DNA polymerases in Ig hypermutation. *Trends Immunol.* 26:215–220. http://dx.doi.org/10.1016/j.it.2005.02.008

Doseth, B., T. Visnes, A. Wallenius, I. Ericsson, A. Sarno, H.S. Pettersen, A. Flatberg, T. Catterall, G. Slupphaug, H.E. Krokan, and B. Kavli. 2011. Uracil-DNA glycosylase in base excision repair and adaptive immunity: species differences between man and mouse. *J. Biol. Chem.* 286:16669–16680. http://dx.doi.org/10.1074/jbc.M111.230052

Faili, A., S. Aoufouchi, Q. Guéranger, C. Zober, A. Léon, B. Bertocci, J.C. Weill, and C.A. Reynaud. 2002. AID-dependent somatic hypermutation occurs as a DNA single-strand event in the BL2 cell line. *Nat. Immunol.* 3:815–821. http://dx.doi.org/10.1038/ni826

Fischer, J.A., S. Muller-Weeks, and S. Caradonna. 2004. Proteolytic degradation of the nuclear isoform of uracil-DNA glycosylase occurs during the S phase of the cell cycle. *DNA Repair (Amst.)*. 3:505–513. http://dx.doi.org/10.1016/j.dnarep.2004.01.012

Fukushima, T., M. Takata, C. Morrison, R. Araki, A. Fujimori, M. Abe, K. Tatsumi, M. Jasin, P.K. Dhar, E. Sonoda, et al. 2001. Genetic analysis of the DNA-dependent protein kinase reveals an inhibitory role of Ku in late S-G2 phase DNA double-strand break repair. *J. Biol. Chem.* 276:44413–44418. http://dx.doi.org/10.1074/jbc.M106295200

Gallant, P., and E.A. Nigg. 1992. Cyclin B2 undergoes cell cycle-dependent nuclear translocation and, when expressed as a non-destructible mutant, causes mitotic arrest in HeLa cells. *J. Cell Biol.* 117:213–224. http://dx.doi.org/10.1083/jcb.117.1.213

Guikema, J.E., E.K. Linehan, D. Tsuchimoto, Y. Nakabeppu, P.R. Strauss, J. Stavnezer, and C.E. Schrader. 2007. APE1- and APE2-dependent DNA breaks in immunoglobulin class switch recombination. *J. Exp. Med.* 204:3017–3026. http://dx.doi.org/10.1084/jem.20071289

Hagen, L., B. Kavli, M.M. Sousa, K. Torseth, N.B. Liabakk, O. Sundheim, J. Pena-Diaz, M. Otterlei, O. Hørning, O.N. Jensen, et al. 2008. Cell cycle-specific UNG2 phosphorylations regulate protein turnover,

activity and association with RPA. *EMBO J.* 27:51–61. http://dx.doi.org/10.1038/sj.emboj.7601958

Hasham, M.G., N.M. Donghia, E. Coffey, J. Maynard, K.J. Snow, J. Ames, R.Y. Wilpan, Y. He, B.L. King, and K.D. Mills. 2010. Widespread genomic breaks generated by activation-induced cytidine deaminase are prevented by homologous recombination. *Nat. Immunol.* 11:820–826. http://dx.doi.org/10.1038/ni.1909

Hevroni, D., and Z. Livneh. 1988. Bypass and termination at apurinic sites during replication of single-stranded DNA in vitro: a model for apurinic site mutagenesis. *Proc. Natl. Acad. Sci. USA.* 85:5046–5050. http://dx.doi.org/10.1073/pnas.85.14.5046

Hodgkin, P.D., J.H. Lee, and A.B. Lyons. 1996. B cell differentiation and isotype switching is related to division cycle number. *J. Exp. Med.* 184:277–281. http://dx.doi.org/10.1084/jem.184.1.277

Holst, J., A.L. Szymczak-Workman, K.M. Vignali, A.R. Burton, C.J. Workman, and D.A. Vignali. 2006. Generation of T-cell receptor retrogenic mice. *Nat. Protoc.* 1:406–417. http://dx.doi.org/10.1038/nprot.2006.61

Imai, K., G. Slupphaug, W.I. Lee, P. Revy, S. Nonoyama, N. Catalan, L. Yel, M. Forveille, B. Kavli, H.E. Krokan, et al. 2003. Human uracil-DNA glycosylase deficiency associated with profoundly impaired immunoglobulin class-switch recombination. *Nat. Immunol.* 4:1023–1028. http://dx.doi.org/10.1038/ni974

Jansen, J.G., P. Langerak, A. Tsaalbi-Shtylik, P. van den Berk, H. Jacobs, and N. de Wind. 2006. Strand-biased defect in C/G transversions in hypermutating immunoglobulin genes in Rev1-deficient mice. *J. Exp. Med.* 203:319–323. http://dx.doi.org/10.1084/jem.20052227

Jolly, C.J., A.J. Cook, and J.P. Manis. 2008. Fixing DNA breaks during class switch recombination. *J. Exp. Med.* 205:509–513. http://dx.doi.org/10.1084/jem.20080356

Kavli, B., O. Sundheim, M. Akbari, M. Otterlei, H. Nilsen, F. Skorpen, P.A. Aas, L. Hagen, H.E. Krokan, and G. Slupphaug. 2002. hUNG2 is the major repair enzyme for removal of uracil from U:A matches, U:G mismatches, and U in single-stranded DNA, with hSMUG1 as a broad specificity backup. *J. Biol. Chem.* 277:39926–39936. http://dx.doi.org/10.1074/jbc.M207107200

Li, Z., D.I. Dordai, J. Lee, and S. Desiderio. 1996. A conserved degradation signal regulates RAG-2 accumulation during cell division and links V(D)J recombination to the cell cycle. *Immunity.* 5:575–589. http://dx.doi.org/10.1016/S1074-7613(00)80272-1

Liu, M., J.L. Duke, D.J. Richter, C.G. Vinuesa, C.C. Goodnow, S.H. Kleinstein, and D.G. Schatz. 2008. Two levels of protection for the B cell genome during somatic hypermutation. *Nature.* 451:841–845. http://dx.doi.org/10.1038/nature06547

Mizuta, R., M. Mizuta, S. Araki, and D. Kitamura. 2002. RAG2 is down-regulated by cytoplasmic sequestration and ubiquitin-dependent degradation. *J. Biol. Chem.* 277:41423–41427. http://dx.doi.org/10.1074/jbc.M206605200

Mol, C.D., A.S. Arvai, R.J. Sanderson, G. Slupphaug, B. Kavli, H.E. Krokan, D.W. Mosbaugh, and J.A. Tainer. 1995. Crystal structure of human uracil-DNA glycosylase in complex with a protein inhibitor: protein mimicry of DNA. *Cell.* 82:701–708. http://dx.doi.org/10.1016/0092-8674(95)90467-0

Muramatsu, M., K. Kinoshita, S. Fagarasan, S. Yamada, Y. Shinkai, and T. Honjo. 2000. Class switch recombination and hypermutation require activation-induced cytidine deaminase (AID), a potential RNA editing enzyme. *Cell.* 102:553–563. http://dx.doi.org/10.1016/S0092-8674(00)00078-7

Nakamura, J., and J.A. Swenberg. 1999. Endogenous apurinic/apyrimidinic sites in genomic DNA of mammalian tissues. *Cancer Res.* 59:2522–2526.

Nilsen, H., I. Rosewell, P. Robins, C.F. Skjelbred, S. Andersen, G. Slupphaug, G. Daly, H.E. Krokan, T. Lindahl, and D.E. Barnes. 2000. Uracil-DNA glycosylase (UNG)-deficient mice reveal a primary role of the enzyme during DNA replication. *Mol. Cell.* 5:1059–1065. http://dx.doi.org/10.1016/S1097-2765(00)80271-3

Ordinario, E.C., M. Yabuki, R.P. Larson, and N. Maizels. 2009. Temporal regulation of Ig gene diversification revealed by single-cell imaging. *J. Immunol.* 183:4545–4553. http://dx.doi.org/10.4049/jimmunol.0900673

Otterlei, M., E. Warbrick, T.A. Nagelhus, T. Haug, G. Slupphaug, M. Akbari, P.A. Aas, K. Steinsbekk, O. Bakke, and H.E. Krokan. 1999. Post-replicative base excision repair in replication foci. *EMBO J.* 18:3834–3844. http://dx.doi.org/10.1093/emboj/18.13.3834

Peled, J.U., F.L. Kuang, M.D. Iglesias-Ussel, S. Roa, S.L. Kalis, M.F. Goodman, and M.D. Scharff. 2008. The biochemistry of somatic hypermutation. *Annu. Rev. Immunol.* 26:481–511. http://dx.doi.org/10.1146/annurev.immunol.26.021607.090236

Petersen, S., R. Casellas, B. Reina-San-Martin, H.T. Chen, M.J. Difilippantonio, P.C. Wilson, L. Hanitsch, A. Celeste, M. Muramatsu, D.R. Pilch, et al. 2001. AID is required to initiate Nbs1/gamma-H2AX focus formation and mutations at sites of class switching. *Nature.* 414:660–665. http://dx.doi.org/10.1038/414660a

Pines, J., and T. Hunter. 1994. The differential localization of human cyclins A and B is due to a cytoplasmic retention signal in cyclin B. *EMBO J.* 13:3772–3781.

Rada, C., J.M. Di Noia, and M.S. Neuberger. 2004. Mismatch recognition and uracil excision provide complementary paths to both Ig switching and the A/T-focused phase of somatic mutation. *Mol. Cell.* 16:163–171. http://dx.doi.org/10.1016/j.molcel.2004.10.011

Robertson, A.B., A. Klungland, T. Rognes, and I. Leiros. 2009. DNA repair in mammalian cells: Base excision repair: the long and short of it. *Cell. Mol. Life Sci.* 66:981–993. http://dx.doi.org/10.1007/s00018-009-8736-z

Sakaue-Sawano, A., H. Kurokawa, T. Morimura, A. Hanyu, H. Hama, H. Osawa, S. Kashiwagi, K. Fukami, T. Miyata, H. Miyoshi, et al. 2008. Visualizing spatiotemporal dynamics of multicellular cell-cycle progression. *Cell.* 132:487–498. http://dx.doi.org/10.1016/j.cell.2007.12.033

Saribasak, H., R.W. Maul, Z. Cao, R.L. McClure, W. Yang, D.R. McNeill, D.M. Wilson III, and P.J. Gearhart. 2011. XRCC1 suppresses somatic hypermutation and promotes alternative nonhomologous end joining in Igh genes. *J. Exp. Med.* 208:2209–2216. http://dx.doi.org/10.1084/jem.20111135

Schrader, C.E., J.E. Guikema, E.K. Linehan, E. Selsing, and J. Stavnezer. 2007. Activation-induced cytidine deaminase-dependent DNA breaks in class switch recombination occur during G1 phase of the cell cycle and depend upon mismatch repair. *J. Immunol.* 179:6064–6071.

Sharbeen, G., A.J. Cook, K.K. Lau, J. Raftery, C.W. Yee, and C.J. Jolly. 2010. Incorporation of dUTP does not mediate mutation of A:T base pairs in Ig genes in vivo. *Nucleic Acids Res.* 38:8120–8130. http://dx.doi.org/10.1093/nar/gkq682

Shen, H.M., A. Tanaka, G. Bozek, D. Nicolae, and U. Storb. 2006. Somatic hypermutation and class switch recombination in Msh6(−/−)Ung(−/−) double-knockout mice. *J. Immunol.* 177:5386–5392.

Stavnezer, J., J.E. Guikema, and C.E. Schrader. 2008. Mechanism and regulation of class switch recombination. *Annu. Rev. Immunol.* 26:261–292. http://dx.doi.org/10.1146/annurev.immunol.26.021607.090248

Storb, U., H.M. Shen, and D. Nicolae. 2009. Somatic hypermutation: processivity of the cytosine deaminase AID and error-free repair of the resulting uracils. *Cell Cycle.* 8:3097–3101. http://dx.doi.org/10.4161/cc.8.19.9658

Wu, X., and J. Stavnezer. 2007. DNA polymerase β is able to repair breaks in switch regions and plays an inhibitory role during immunoglobulin class switch recombination. *J. Exp. Med.* 204:1677–1689. http://dx.doi.org/10.1084/jem.20070285

Xue, K., C. Rada, and M.S. Neuberger. 2006. The in vivo pattern of AID targeting to immunoglobulin switch regions deduced from mutation spectra in msh2$^{-/-}$ ung$^{-/-}$ mice. *J. Exp. Med.* 203:2085–2094. http://dx.doi.org/10.1084/jem.20061067

Yabuki, M., M.M. Fujii, and N. Maizels. 2005. The MRE11-RAD50-NBS1 complex accelerates somatic hypermutation and gene conversion of immunoglobulin variable regions. *Nat. Immunol.* 6:730–736. http://dx.doi.org/10.1038/ni1215